170-MHz Electrodeless Quartz Crystal Microbalance Biosensor: Capability and Limitation of Higher Frequency Measurement

Hirotsugu Ogi,[*,†,§] Hironao Nagai,[†] Yuji Fukunishi,[†] Masahiko Hirao,[†] and Masayoshi Nishiyama[‡]

Graduate School of Engineering Science, Osaka University, Machikaneyama 1-3, Toyonaka, Osaka 560-8531, Japan, and Central Workshop, Osaka University, Machikaneyama 1-2, Toyonaka, Osaka 560-0043, Japan

E-mail: ogi@me.es.osaka-u.ac.jp

Abstract

We develop a high sensitive quartz-crystal microbalance (QCM) biosensor with a fundamental resonance frequency of 170 MHz. A naked AT-cut quartz plate of 9.7 μm thick is set in a sensor cell. Its shear vibration is excited by the line wire and the vibration signals are detected by the other line wire, achieving the noncontacting measurement of the resonance frequency. The mass sensitivity of the 170 MHz QCM biosensor is 15 pg/(cm^{2}Hz), which is better than that of a conventional 5 MHz QCM by three orders of magnitude. Its high sensitivity is confirmed by detecting human immunoglobulin G (hIgG) via Staphylococcus protein A immobilized nonspecifically on both surfaces of the quartz plate. The detection limit is 0.5 pM. Limitation of the high-frequency QCM measurement is then theoretically discussed

[†]Graduate School of Engineering Science
[‡]Central Workshop, Osaka University, Machikaneyama 1-2, Toyonaka, Osaka 560-0043, Japan
[§]PRESTO, JST. 4-1-8 Honcho, Kawaguchi, Saitama, Japan

with a continuum mechanics model for a plate with point masses connected by elastic springs. The result indicates that a QCM measurement will break down at frequencies one-order-of-magnitude higher than the local resonance frequency at specific binding cites.

Introduction

Quartz-crystal microbalance (QCM) biosensor allows label-free and real-time detection of biomolecules in liquid through the change in resonance frequency of a quartz-plate oscillator. Injecting an analyte into a sensor cell, where the oscillator is located, target proteins are adsorbed on receptor proteins immobilized on the oscillator surfaces, resulting in the increase in the effective mass of the resonator and in the decrease in the resonance frequency. The frequency change is directly related with the kinetics of the recognition reaction at higher frequencies, and when the reaction occurs with the pseudo-first-order manner, the frequency changes exponentially; the exponential coefficient depends on the concentration of the target protein in the analyte and the affinity between the interacting proteins.[1–3] (The amount of water coupled to adsorbed proteins substantially contributes to the frequency change and this effect has to be taken into account in the determination of the affinity.[4]) The sensitivity and usability of a QCM biosensor are nearly the same as those of surface-plasmon-resonance biosensors,[5–7] which are also label-free biosensors, allowing the real-time monitoring of binding reactions between biomolecules.

QCM is a mass-sensitive biosensor, and its sensitivity increases as the oscillator mass decreases. Keeping the active sensing area unchanged, the reduction of the oscillator mass is achieved by thinning the oscillator, leading to the increase in the fundamental resonance frequency f_1. Because the change in the resonance frequency caused by the adsorption of proteins is proportional to f_1^2,[8] the reduction of the oscillator thickness significantly increases the QCM sensitivity.

Furthermore, a high-frequency QCM measurement is needed for quantitative analysis. The viscosity effect varies the resonance frequency[9,10] as well as the mass loading effect, making the quantitative evaluation of the adsorbed protein mass complicated. Low-frequency QCM measure-

ments are easily affected by the viscosity effect, and the simultaneous measurement of resonance frequency and dissipation has been performed for compensating for the frequency change due to the viscosity effect.[11–16] Because the viscosity effect becomes insignificant compared with the mass loading effect at high frequencies,[17,18] a higher frequency QCM measurement is desired.

The most previous studies with QCM biosensors used 5 or 10 MHz fundamental resonance frequency.[19–22] However, higher-frequency QCM systems were recently developed as reviewed by Cooper and Singleton.[23] Natesan *et al.*[24] used 16.5 MHz QCM for detecting staphylococcal enterotoxin B and achieved the detection limit of 25 ng/mL. Furusawa *et al.*[25,26] developed a 27 MHz QCM system to increase the sensitivity, although their method cannot adopt a flow-injection-analysis system. Uttenthaler *et al.* developed high frequency QCMs with resonant frequencies from 39 to 110 MHz in the liquid.[27]

Almost all quartz plates used in these previous studies needed electrodes on both surfaces for applying the effective electric field. However, gold electrodes deteriorate the mass sensitivity because of much higher mass density of gold than that of quartz, and this influence becomes marked as the fundamental resonance frequency increases.[28] Furthermore, the active sensing region is restricted near the center region where the electrodes are attached, and a large part of surface area remains inactive, deteriorating the sensitivity. Thus, the electrodeless QCM biosensors are obviously preferable.

We recently developed a wireless-electrodeless QCM (WE-QCM) system, where a naked AT-cut quartz plate is driven by the line antenna or the flat-coil antenna contactlessly,[17] and achieved high frequency QCMs with fundamental resonance frequencies of 55 MHz[29,30] and 85 MHz.[31] Here, we develop even higher frequency QCM system with a 170-MHz fundamental resonance frequency using a 9.7-μm thick blank AT-cut quartz plate, and evaluate its sensitivity using the binding reaction between staphylococcus aureus protein A (SPA) and human immunoglobulin G (hIgG). SPA is immobilized on both surfaces of the quartz plate via the nonspecific adsorption, where the analyte containing hIgG molecules are injected.

We then study the limitation of higher frequency QCM. The mass loading effect arises when the

adsorbed proteins move with the crystal oscillator. If the binding between the receptor and target proteins is weak, the adsorbed molecules fail to follow the crystal movement and cannot contribute to the additional mass in the resonator system. Thus, a break down would occur when the QCM frequency is beyond a critical value, and we investigate this phenomenon using a vibrational model consisting of a continuum plate and masses connected with the plate by elastic springs.

Experimental Section

We use a 9.7-μm electrodeless AT-cut quartz plate with 2 mm diameter. Both surfaces of the quartz plate were carefully mechanical-polished to obtain smooth surfaces with surface roughness of R_a <0.5 nm. The quartz plate is set in the handmade sensor cell as shown in Fig. 1 after the immobilization of the receptor protein. The edge part of the quartz plate, about 3% of the whole area, is lightly sandwiched by 1-mm thick silicon rubber gaskets.

The sensor cell is located in the temperature controlled box to maintain the solution temperature at 37 °C. The homebuilt flow-injection system[29] is used for monitoring the frequency change during the binding reaction. The carrier solution is a phosphate-buffer solution (PBS) with ph 7.4, and the flow rate is 500 μL/min, which is much larger than that used in conventional QCM flow-injection measurements ($\sim$ 50 μL/min). The larger flow rate is preferable because the motion of proteins in liquid due to Brownian motion is insignificant compared with the motion cause by the flow.[28] The length ($\sim$20 mm) and thickness ($\sim$2 mm) of the flow channel are larger enough than those of the crystal, and we expect that the solution flows near upside and downside of the crystal are identical.

We use two line antennas for generation and detection of the pure shear vibration contactlessly as shown in Fig. 1. These antennas and a thin foil for grounding are embedded in the bottom and top Teflon blocks, respectively. We apply the burst signal near the resonance frequency ($\sim$ 170 MHz) to the generation antenna to cause the quasistatic electric field along the thickness direction of the quartz plate. After the excitation, the detection line antenna receives the reverberating

signals of the crystal, which are fed to the superheterodyne phase-sensitive detector (RITEC Inc. model SNAP 1-200 MHz). A scan of the driving burst frequency yields a resonance peak as shown in Fig. 2, and the Lorentzian-function fitting provides the resonance frequency from the center axis. (Sometimes, the resonance peak shape was not like a Lorentzian function. However, the Lorentzian-function fitting worked well to determine the center axis accurately, because the peak showed good symmetry about the center axis.) After the resonance frequency becomes sufficiently stable, we monitor the phase of the received signal at the fixed frequency to determine the resonance-frequency change from the linear relationship between the phase and frequency near the resonance frequency (see the broken line in Fig. 2). This procedure determines the resonance frequency every 3 ms with the fluctuation smaller than 1.0×10^{-6}. We made 500-times averaging for the stable measurement, and obtained the resonance frequency every $\sim$1.0 s. The standard deviation of the frequency fluctuation during the flow of the carrier solution is about 1×10^{-7}($\sim$15 Hz) for 1 h.

To demonstrate higher sensitivity of the 170 MHz electrodeless QCM biosensor, we perform to detect hIgG via SPA using 330, 30, and 9.7 μm thick electrodeless quartz plates. (Their fundamental resonance frequencies are 5, 55, and 170 MHz, respectively). Because SPA and hIgG bind each other with a high affinity ($K_D = \sim 10^{-7} - 10^{-11}$ M)[18,32–34] and SPA directly adsorbs on the blank quartz surface with a relatively higher affinity ($K_D \sim 10^{-7}$ M),[30] we detect hIgG via SPA nonspecifically immobilized on the quartz surfaces. Thus, no bridging material such as a self-assembled monolayer is needed, and the sensor chips can be used semipermanently by washing them with a strong acid solution. The hIgG concentration in PBS is varied between 0.5 pM and 50 nM.

The sensor chips were first cleaned in a piranha solution (98%H_2SO_4:33%H_2O_2=7:3) for 30 min and rinsed by the ultrapure water three times. They were then immersed in a 400 μg/mL SPA/PBS solution for 12 h at 4 °C. After rinsing with the PBS solution, the sensor chips were set in the sensor cell for the flow-injection measurement.

hIgG was purchased from Athens Research and Technology, Inc. (product num. 16-16-090707;

purity ∼95%). SPA was from Zymed Laboratories, Inc. (product num. 10-1100; purity ∼98%).

Results

Figure 3(a) shows the typical frequency changes during the binding reaction between SPA and hIgG caused by the injection of the hIgG solution. As the fundamental resonance frequency increases, the frequency decrement increases drastically. Figure 3(b) compares the amount of the frequency change in the logarithmic scale. Figure 4 shows the binding curves for the independent injections of 0.5 pM hIgG solution as well as the baseline.

Discussion

Obviously from Fig. 3, the sensitivity of the 170 MHz QCM biosensor is much higher than those of conventional 5 MHz QCM biosensors. We see the three-orders-of-magnitude increase in the frequency change for the 170 MHz QCM. According to the Sauerbrey equation, the relationship between the adsorption mass m_p on quartz surfaces and the frequency change Δf is obtained by[8]

$$\frac{m_p}{A_e} = C_{\mathrm{Q}}|\Delta f|, \tag{1}$$

$$C_{\mathrm{Q}} = \frac{\sqrt{\mu_q \rho_q}}{2N}\frac{A_q}{A_e}\cdot\frac{1}{f_1^2} \tag{2}$$

Where N is the overtone number and equals to unity here. A_e and A_q are the effective sensing area and the one-sided surface area of the crystal, respectively. Their ratio A_q/A_e is directly related with the QCM sensitivity, and it is larger than 1 for a conventional QCM using a single side of a quartz plate, while it nearly equals 0.5 for the wireless-electrodeless QCM because almost whole surfaces can be used. ρ_q and μ_q are the mass density and the shear modulus of the crystal. The coefficient C_{Q} expresses the QCM sensitivity, which becomes smaller for a high-sensitive QCM biosensor. C_{Q} equals 7.58 pg/(cm^{2}Hz) for a 170 MHz electrodeless QCM, which is three-orders-of-magnitude smaller than that of a conventional 5-MHz single-side QCM (C_{Q}=17500 pg/(cm^{2}Hz)).

The baseline stability is also an important parameter governing the detection limit. The frequency fluctuation of our handmade QCM biosensor is not great at present ($\sim$15 Hz) compared with the low frequency QCM biosensors ($<\sim$0.1 Hz). We use a flow rate larger than that in the conventional QCM by a factor 10, which deteriorates the frequency stability, although the larger flow rate enhances the adsorption reaction, contributing to the larger frequency change.[28] Thus, the flow rate and the frequency stability pose a trade-off relationship. The baseline problem, however, occurs when we monitor the biding reaction of very low concentration solution. But, such a reaction takes a longer time, and we can use a larger number of averaging for acquiring the frequency to making the baseline more stable. By taking 5000 averaging for one measurement, for example, the frequency fluctuation decreased to be 5 Hz, although the time needed for one measurement increases to be 10 s. Quicker measurement is possible to improve the electronics, which is however beyond the purpose of this study. Thus, the baseline stability will be improved in our future study.

Figure 4 shows the independent measurements for the injection of 0.5 pM hIgG solution. Because the immobilization of SPA on quartz was made through the nonspecific adsorption, the binding curves of the three measurements were not so identical. (The repeatability of the nonspecific adsorption deteriorates compared with the specific adsorption or covalent binding.[30]) However, the resonance frequency shows a distinct descent after the arrival of the hIgG solution, confirming that hIgG in such a low-concentration solution is successfully detected even with the nonspecifically immobilized receptors. The detection limit for the current binding system is 0.5 pM.

Assuming the pseudo-first-order reaction, the exponential coefficient of the binding curve, α, is related to the concentration of the analyte C_A, the association-rate constant k_a, and the dissociation-rate constant k_d as

$$\alpha = k_a C_A + k_d \tag{3}$$

The equilibrium dissociation constant K_D defined by k_d/k_a is obtained by plotting C_A versus α and calculating the regression line.[28] We thus determined the *average* affinity between SPA and

hIgG to be 1.7×10^{-8} M in the wide bulk concentration range used here. This value is equivalent to the values determined by the radiolabeled affinity method.[32] When we estimate the equilibrium frequency change Δf_{eq} from this affinity value, Δf_{eq} would be $\sim$10 Hz for the injection of the 0.5 pM solution, which is much smaller than the observed frequency change ($>$1 kHz) in Fig. 4. This is because that the affinity between SPA and hIgG is significantly concentration dependent,[34] and the K_D value drastically decreases at a low concentration of hIgG solution.[18] For example, $K_D = 1.7 \times 10^{-11}$ M in the concentration range of $C_A <$700 pM,[18] and using this value, we obtain $\Delta f_{eq} \sim$2 kHz at C_A=0.5 pM. This value is, thus, consistent with the measurement in Fig. 4, supporting the detection of hIgG even in the low concentration solution.

Equations (1) and (2) indicate that the frequency change Δf is proportional to the square of fundamental resonance frequency f_1, and the measurement in Fig. 3 quantitatively agree with this relationship: The measured Δf for the injection of 50 nM hIgG solution are 62, 7450, and 61000 Hz for 5, 55, and 170 MHz QCMs, respectively, yielding the linear relationship between f_1^2 and Δf with the coefficient of correlation of $|R| =$0.9999. This agreement of the measurement with the Sauerbrey equation is attributed to using the electrodeless sensor chips. Figure 5 shows the influences of the gold electrode on quartz surfaces on the frequency change when 1-nm thick hIgG layers are adsorbed on both surfaces. (The theoretical calculation was made for a five layer morel, consisting of the middle quartz layer, sandwiching gold layers, and outer protein layers. The details of the calculation appear in the previous study.[28]) It should be noted that the frequency change is significantly affected by the presence of the electrode. For example, a 200 nm thick gold electrode lowers the amount of the frequency changes for 170 and 55 MHz QCMs by 45% and 18%, respectively, while it hardly affects the sensitivity of a 5 MHz QCM. Because of much larger mass density of gold than quartz and the maximum accelerated velocity at the surface, the inertia resistance caused by the electrode becomes significant, making the Sauerbrey equation invalid for a high-frequency QCM with the electrode. Thus, the electrodeless approach is essential not only for a high sensitive QCM but also for a quantitative analysis with the Sauerbrey equation.

Finally, we analyze the detection limit of a high-frequency QCM biosensor. The Sauerbrey

equation indicates that the QCM sensitivity increase as the fundamental resonance frequency increases. However, when the binding proteins cannot follow the movement of the oscillator, they fail to contribute to the effective mass in the resonator system. Thus, there is a critical frequency, beyond which the adsorbed proteins cannot be detected.

For this analysis, we propose a model as shown in Fig. 6, assuming that the receptor proteins are rigidly immobilized on quartz surfaces and the interaction with the binding protein can be replaced by an elastic spring with a spring constant, regarding the binding protein as a point mass: The spring constant and the point mass per unit area are denoted by $\tilde{k}$ and $\tilde{m}$, respectively. The displacement of the point mass u_p is measured from the global origin. Because the proteins on surfaces affect little the displacement distribution in the quartz plate, we assume the same displacement distribution in the quartz u_q as that of the free vibration state. Thus, the displacements take the forms of

$$u_q = A\sin\left(\frac{\pi z}{t_q}\right)\mathrm{e}^{j\omega t}, \tag{4}$$

$$u_p = B\mathrm{e}^{j\omega t} \tag{5}$$

where A and B denote the amplitudes for u_q and u_p, respectively. t_q denotes the thickness of the quartz plate. We use Hamilton's principle for determining resonance frequencies of the resonator system, where the energy of the system should be minimized with respect to the unknown parameters A and B. The energy of the system U per unit area on the surface, consisting of the kinetic energy and the strain energy, is obtained as

$$U = \left\{\frac{\pi^2\mu_q}{4t_q}A^2 + \tilde{k}(A+B)^2\right\} - \omega^2\left\{\frac{t_q\rho_q}{4}A^2 - \tilde{m}B^2\right\} \tag{6}$$

The first bracket denotes the strain energy and the second one the kinetics energy per unit area.

Partial differentiations of U with respect to A and B yield

$$\begin{bmatrix} \pi^2\mu_q/2t_q + 2\tilde{k} - t_q\rho_q\omega^2/2 & 2\tilde{k} \\ \tilde{k} & (\tilde{k} - \tilde{m}\omega^2) \end{bmatrix} \begin{bmatrix} A \\ B \end{bmatrix} = \begin{bmatrix} \Gamma \end{bmatrix} \begin{bmatrix} A \\ B \end{bmatrix} = \begin{bmatrix} 0 \\ 0 \end{bmatrix} \tag{7}$$

Thus, by solving the equation, det[Γ]=0, with respect to ω, we have the resonance frequencies of the system. (There are two solutions, and we focus on the one close to the Sauerbrey prediction. The other solution expresses a mode localized at the binding site.) Figure 7 shows the fractional change in the resonance frequency calculated by varying the local resonance frequency at a single protein pair ($\omega_{\text{bind}} = \sqrt{\tilde{k}/\tilde{m}}$) in the case that the ratio of the adsorbed protein mass to the quartz mass ($\tilde{m}/(\rho_q t_q)$) equals 1×10^{-5}, a typical case of a QCM measurement. The horizontal axis is normalized by the free-vibration resonance frequency of the quartz plate ($\omega_q = \pi/t_q\sqrt{\mu_q/\rho_q}$). The horizontal broken line is the prediction by the Sauerbrey equation. When ω_{bind} is much higher than ω_q, the analytical solution is identical to the Sauerbrey equation, indicating that the adsorbed protein molecules completely follow the oscillator motion to contribute to the increase in the resonator mass. However, when $\omega_{\text{bind}} << \omega_q$, the adsorbed proteins cannot be recognized as the effective mass, and they will not be detected through the mass-loading effect. Therefore, the QCM frequency has to be lower than ω_{bind}, at least lower by one order of magnitude.

It is not straightforward to estimate the stiffness of the interaction between the proteins. There are, however, some reports on phonon vibrational frequencies of proteins, consisting of large domains. Their lower frequency vibrations for breathing and expansion-contraction modes show larger vibrational amplitudes. The local resonance frequency at the interaction will be approximately identical to those low-frequency and large-amplitude vibrational modes of proteins in the case of the strong binding, otherwise the attractive interaction should be broken because of the large vibrational amplitudes of proteins. The vibration frequencies of breathing modes of IgG domains (V_H, V_L, and C_{HL}) were calculated using the quasi-continuity model[35] to be about 800-1000 GHz. Brown *et al.*[36] detected a low frequency vibration mode at 870 GHz in α-chymotrypsin using laser Raman spectroscopy. Picquart *et al.*[37] estimated the lowest vibration frequency of the heavy and

light chains in an IgG molecule to be 87 and 174 GHz, respectively. Thus, the lowest phonon modes appear at frequencies higher than ∼80 GHz, which is much higher than the fundamental resonance frequency used here (170 MHz). Thus, we expect that the present 170 MHz QCM will detect most binding proteins through the mass loading effect. However, we have to note that as the QCM frequency increases more and the bonding interaction becomes much weaker, the critical frequency point ($\omega_{\text{bind}} < \omega_q$) approaches, and the QCM would be of no use.

Conclusion

We developed a 170 MHz electrodeless QCM system and showed its higher sensitivity than conventional QCMs even with use of nonspecifically adsorbed receptor proteins. hIgG molecules were detected by the SPA molecules, which were immobilized on the naked quartz surface nonspecifically. The amount of the resonance-frequency change caused by the binding reaction between them was three-orders-of-magnitude higher than that of the 5 MHz QCM. The affinity between hIgG and SPA was derived, which agreed with the previously determined values by radioimmunoassay. Because of the wireless-electrodeless nature, the sensor chips can be used semipermanently by washing them with a strong acid. An analytical model was proposed for estimating the critical frequency, beyond which the QCM measurement breaks down. The result indicates that the QCM frequency has to be lower than the local resonance frequency at the binding protein by a factor of 0.1.

Acknowledgement

A part of this study was supported by Life Phenomena and Measurement Analysis, PRESTO, by Japan Science and Technology Agency.

References

(1) Eddowes, M. J. Biosensors. 1987, 3, 1-15.

(2) Ebara, Y.; Itakura, K.; Okahata, Y. Langmuir. 1996, 12, 5165-5170.

(3) Liu, Y.; Yu, X.; Zhao, R.; Shangguan, D.; Bo, Z.; Liu, G. Biosens. Bioelectron. 2003, 19, 9-19.

(4) Bingen, P.; Wang, G.;Steinmetz, N. F.; Rodahl, M.; Richter, R. P. Anal. Chem. 2008, 80, 8880-8890.

(5) Spangler, B. D.; Wilkinson, E. A.; Murphyb, J. T.; Tyler, B. J. Anal. Chim. Acta 2001, 444, 149-161.

(6) Laricchia-Robbio, L.; Revoltella, R. P. Biosens. Bioelectron. 2004, 19,1753-1758.

(7) Su, X.; Zhang, J. Sens. Actuators, B 2004, 100, 309-314.

(8) Sauerbrey, G. Z. Phys. 1959, 155, 206-222.

(9) Kanazawa, K. K.; Gordon, J. G. Anal. Chim. Acta. 1985, 175, 99-105.

(10) Martin, S. J.; Granstaff, V. E.; Frye, G. C. Anal. Chem. 1991, 63, 2272-2281.

(11) Rodahl, M.; Kasemo, B. Sens. Actuat. 1996, 54, 448-456.

(12) Höök, F.; Rodahl, M.; Brzezinski, P.; Kasemo, B. Langmuir 1998, 14, 729-734.

(13) Höök, F.; Kasemo, B.; Nylander, T.; Fant, C.; Sott, K.; Elwing, H. Anal. Chem. 2001, 73, 5796-5804.

(14) Reimhult, E.; Larsson, C.; Kasemo, B.; Höök, F. Anal. Chem. 2004, 76, 7211-7220.

(15) Zong, Y.; Xu, F.; Su, X.; Knoll, W. Anal. Chem. 2008, 80, 5246-5250.

(16) Jonsson, M. P.; Jönsson, P.; Höök, F. Anal. Chem. 2008, 80, 7988-7995.

(17) Ogi, H.; Motohisa, K.; Matsumoto, T.; Hatanaka, K.; Hirao, M. Anal. Chem. 2006. 78, 6903-6909.

(18) Ogi, H.; Motohisa, M.; Hatanaka, K.; Ohmori, T.; Hirao, M.; Nishiyama, M. Biosens. Bioelectron. 2007, 22, 3238-3242.

(19) Muramatsu, H.; Dicks, M. D.; Tamiya, E.; Karube, I. Anal. Chem. 1987, 59, 2760-2763.

(20) Guzmn, E.; Ritacco, H.;Ortega, F.;Svitova, T.;Radke, C. J.;Rubio, R. G. J. Phys. Chem. B 2009, 113, 7128-7137.

(21) Kang, H.; Muramatsu, H. Biosens. Bioelectron. 2009, 24, 1318-1323.

(22) Wang, S.; Milam, J.; Ohlin, A. C.; Rambaran, V. H.;Clark, E.; Ward, W.; Seymour, L.; Casey, W. H.;Holder, A. A.; Miao, W. Anal. Chem. 2009, 81, 4068-4075.

(23) Cooper, M. A.; Singleton, V. T. J. Mol. Recognit. 2007, 20, 154-184.

(24) Natesan, M.; Cooper, M. A.;Tran, J. P;Rivera, V. R.;Poli, M. A. Anal. Chem. 2009, 81, 3896-3902.

(25) Furusawa, H.; Ozeki, T.; Morita, M.; Okahata, Y. Anal. Chem. 2009, 81, 2268-2273.

(26) Furusawa, H.; Komatsu, M.; Okahata, Y. Anal. Chem. 2009, 81, 1841-1847.

(27) Uttenthaler, E.; Schr´aml, M.;Mandel, J.; Drost, S. Biosens. Bioelectron. 2001, 16, 735-743.

(28) Ogi, H.; Fukunishi, Y.; Omori, T.; Hatanaka, K.; Hirao, M.; Nishiyama, M. Anal. Chem. 2008, 80, 5494-5500.

(29) Ogi, H.; Okamoto, K.; Nagai, H.;Fukunishi, Y.; Hirao, M. Anal. Chem. 2009, 81, 4015-4020.

(30) Ogi, H.; Fukunishi, Y.; Nagai, H.; Okamoto, K.; Hirao, M.; Nishiyama, M. Biosens. Bioelectron. 2009, 24, 3148-3152.

(31) Ogi, H.; Ohmori, T.; Hatanaka, K.; Hirao, M.; Nishiyama, M. Jpn. J. Appl. Phys. 2008, 47, 4021-4023.

(32) Kronvall, G.; Quie, P. G. ;Williams, R. C. Jr. J. Immunol. 1970, 104, 273-278.

(33) Hanson, D. C. ; Schumaker, V. N. J. Immunol. 1984, 132, 1397-1409.

(34) Kessler, S. W. J. Immunol. 1975, 115, 1617-1624.

(35) Chou, K. Biopolymers. 1987, 26, 285-295.

(36) Brown, K. G.; Erfurth, S. C.;Small, E. W.;Peticolas, W. L. Proc. Nat. Acad. Sci. USA. 1972, 69, 1467-1469.

(37) Picquart, M.; Haro-Poniatowski, E.; Morhange, J. F.; Jouanne, M.; Kanehisa, M. Biopolymers. 2000, 53, 342-349.

Figure Caption

Fig. 1 Top and side views of the homebuilt sensor cell. The two antenna wires are embedded in the bottom Teflon block, and the thin grounding foil is in the top Teflon block. The silicon rubbers sandwiches the edge of a 10-μm thick quartz plate.

Fig. 2 Resonance spectrum (solid line) and the phase change (broken line) of a 9.7 μm thick AT-cut quartz located in PBS measured by the line antennas contactlessly. Both quartz surfaces are exposed to the solution.

Fig. 3 (Color online)(a)Typical frequency changes caused by the injection of the hIgG solution detected by three electrodeless QCMs. (b)Logarithmic resonance-frequency change during the injection of the hIgG solution. For the 5 pM hIgG solution, two independent measurements are shown.

Fig. 4 (Color online) Resonance frequency changes caused by the injection of 0.5 pM hIgG solution. Three independent measurements are shown.

Fig. 5 Influence of the gold electrode on the amount of the resonance frequency change caused by the adsorption of hIgG layers on both surfaces. The open circles denote the prediction by the Sauerbrey equation and the solid lines are analytical calculation for the five layer model.

Fig. 6 Continuum mechanics model for vibrations of a plate with point masses connected by the elastic springs.

Fig. 7 Dependence of the fractional change in the resonance frequency caused by the adsorption of proteins on the local resonance frequency ω_{bind} at the binding pair (solid line). The horizontal broken line denotes the prediction by the Sauerbrey equation.

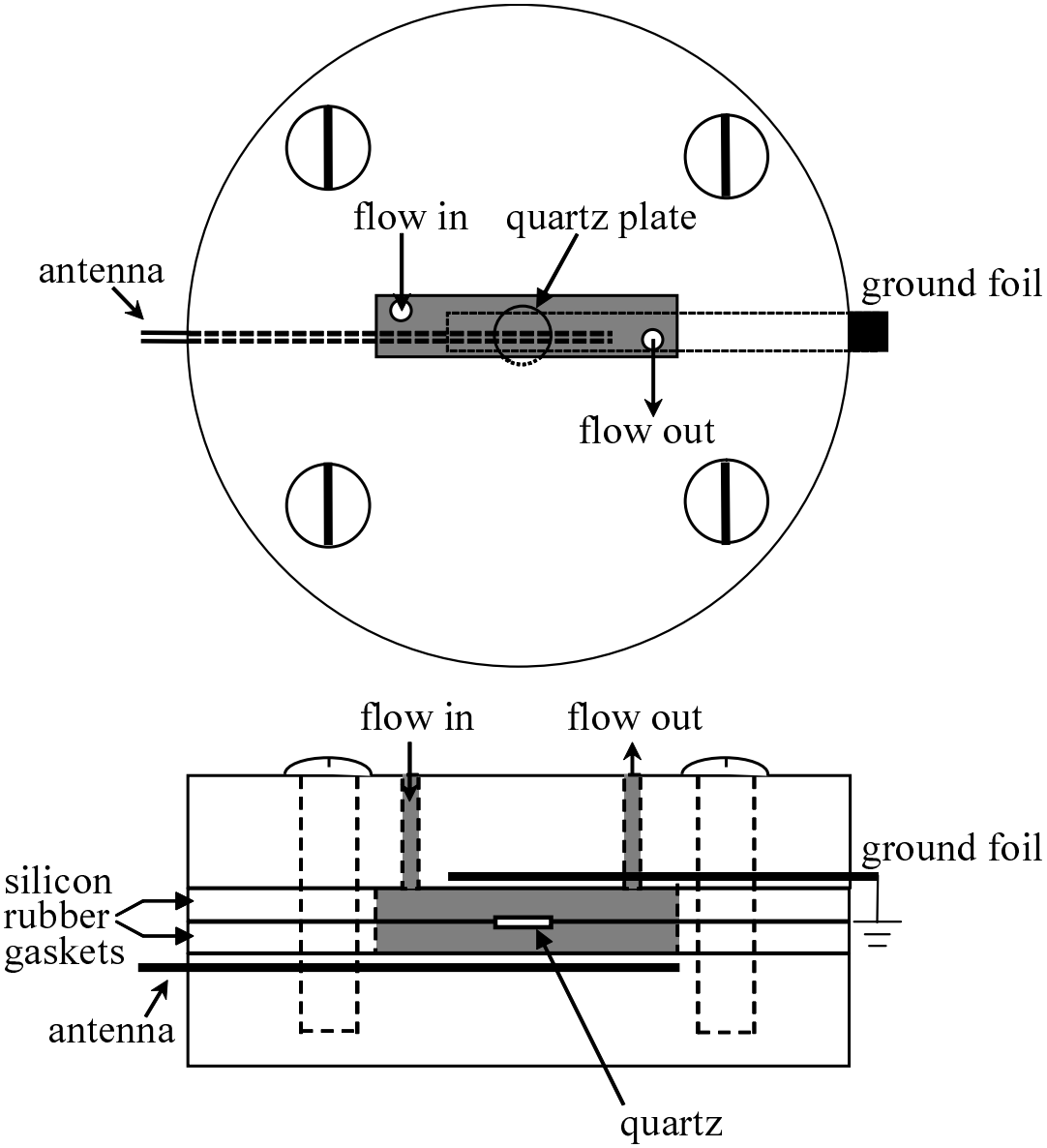
flow in
quartz plate
antenna
ground foil
flow out
flow in
flow out
ground foil
silicon
rubber
gaskets
antenna
quartz

Figure 1:

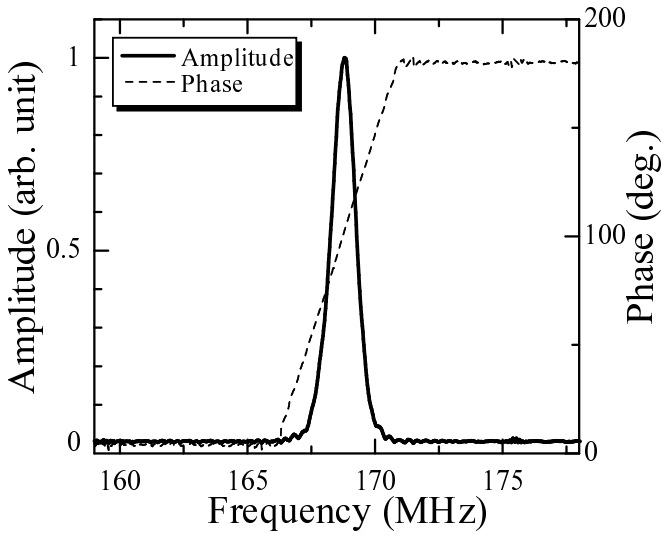
Amplitude
Phase
Amplitude (arb. unit)
Phase (deg.)
Frequency (MHz)
0
0.5
1
0
100
200
160
165
170
175

Figure 2:

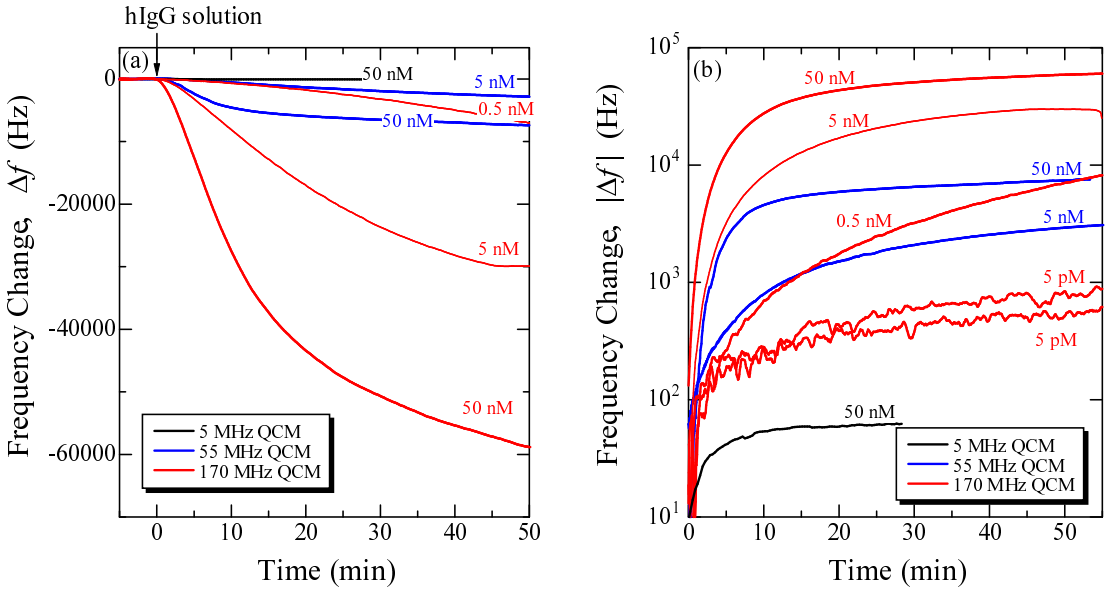
hIgG solution
(a)
0
-20000
-40000
-60000
Frequency Change, Δf (Hz)
50 nM
5 nM
0.5 nM
50 nM
5 nM
50 nM
5 MHz QCM
55 MHz QCM
170 MHz QCM
0
10
20
30
40
50
Time (min)
(b)
10^5
10^4
10^3
10^2
10^1
Frequency Change, |Δf| (Hz)
50 nM
5 nM
50 nM
0.5 nM
5 nM
5 pM
5 pM
50 nM
5 MHz QCM
55 MHz QCM
170 MHz QCM
0
10
20
30
40
50
Time (min)

Figure 3:

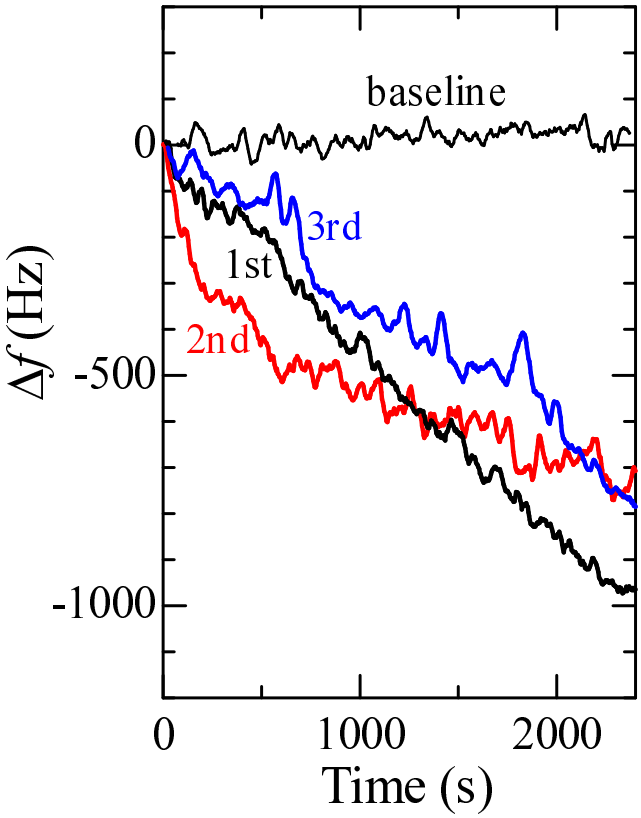

Figure 4:

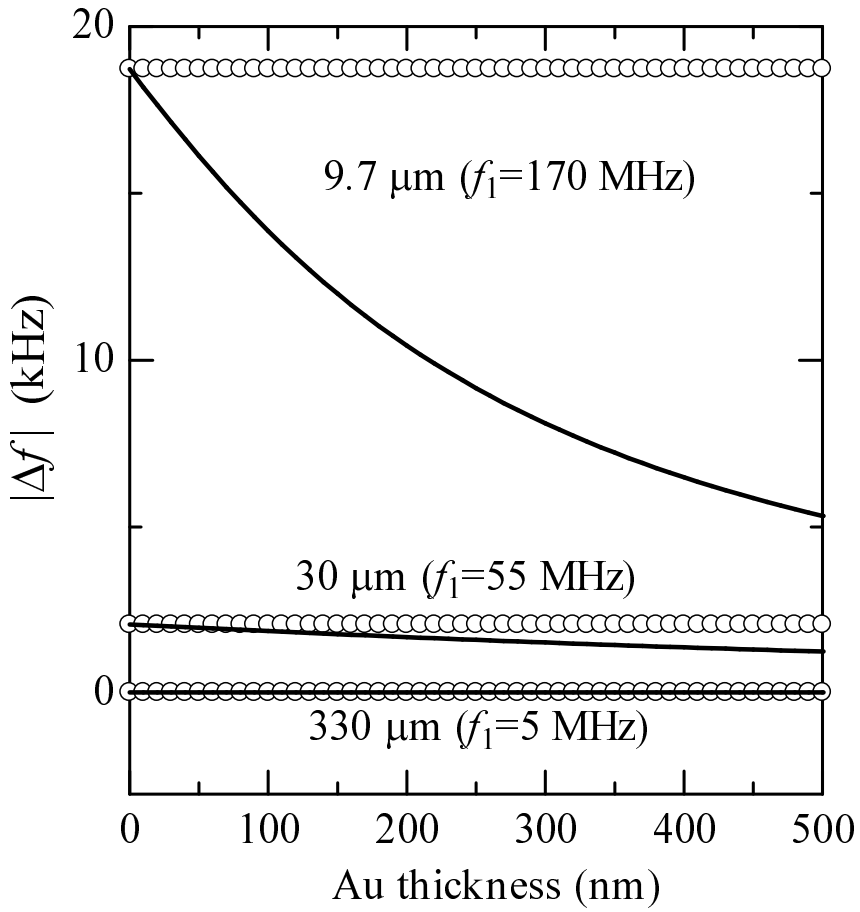
20
10
0
|Δf| (kHz)
9.7 μm (f1=170 MHz)
30 μm (f1=55 MHz)
330 μm (f1=5 MHz)
0
100
200
300
400
500
Au thickness (nm)

Figure 5:

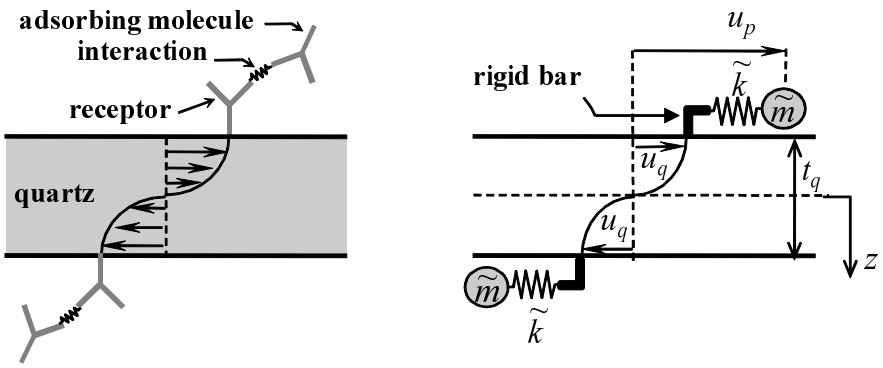
adsorbing molecule
interaction
receptor
quartz
u_p
rigid bar
$\tilde{k}$
$\tilde{m}$
u_q
t_q
u_q
z
$\tilde{m}$
$\tilde{k}$

Figure 6:

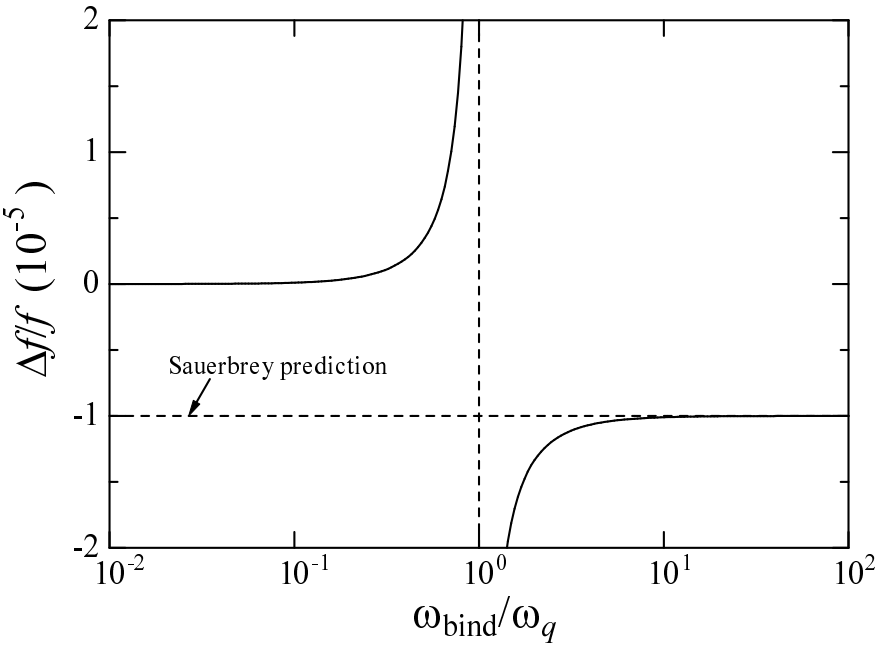
2
1
0
-1
-2
Δf/f (10^-5)
Sauerbrey prediction
10^-2
10^-1
10^0
10^1
10^2
ω_bind/ω_q

Figure 7: